

https://dspace.org/

Exploring the ambient metastability of yttrium substituted Bi2O3 electrolyte materials

Mathias Kiefer; Sikhumbuzo Masina; Caren Billing; Daniel Olds; David Billing

ELSEVIER SCI LTD
https://hdl.handle.net/10539/41810
WOS

Downloaded from a DSpace repository. https://dspace.org/

Ceramics International 50 (2024) 40079–40086

Contents lists available at ScienceDirect

Ceramics International

journal homepage: www.elsevier.com/locate/ceramint

Exploring the ambient metastability of yttrium substituted Bi_2O_3 electrolyte materials

Mathias A. Kiefer [a,c], Sikhumbuzo M. Masina [a,c], Caren Billing [a,c,*], Daniel Olds [b], David G. Billing [a,c]

[a] Molecular Science Institute, School of Chemistry, University of the Witwatersrand, Private Bag X3, Johannesburg, 2050, South Africa
[b] National Synchrotron Light Source II, Brookhaven National Laboratory, PO Box 5000, Upton, NY, 11973, USA
[c] DSI-NRF Centre of Excellence in Strong Materials, University of the Witwatersrand, Private Bag X3, Johannesburg, 2050, South Africa

ARTICLE INFO

Handling Editor: Dr P. Vincenzini

Keywords:
C. Lifetime
C. Chemical properties
E. Fuel cells
Bismuth oxide

ABSTRACT

The phase stability of $(Bi_{1-x}Y_x)_2O_3$ ($0.1 \leq x \leq 0.275$) solid state electrolytes synthesized using the sol-gel method was investigated over prolonged periods under ambient conditions. The cubic polymorph was found to be metastable under ambient conditions, particularly for $0.1 \leq x \leq 0.15$ where significant cubic-to-tetragonal transformation occurred. Spontaneous minor formation of both the rhombohedral polymorph and a bismuth subcarbonate phase was evident across the doping range but with varied reproducibility. Aging was significantly more prevalent for samples that had only been calcined (at 450 °C) as compared to those that were subsequently annealed (at 750 °C). The more highly substituted annealed materials ($0.25 \leq x \leq 0.275$) were initially phase pure cubic and far more stable, yet some rhombohedral and bismuth subcarbonate phase formation was also seen. Although the initial source of carbon which leads to the formation of the subcarbonate phase is not known at this stage, several suggestions are made. Pelletisation with additional sintering, as well as annealing powder samples under an inert atmosphere, was also shown to enhance the long-term phase stability characteristics of the cubic phase. This is the first longer term (over 2 years) ambient phase aging study of substituted bismuth oxides.

1. Introduction

The phase stability of the face-centred cubic δ-phase bismuthates has been the subject of substantial research in context of these materials as solid oxide fuel cell (SOFC) electrolytes. Early on Harwig [1], Harwig and Gerards [2], and Rao et al. [3], found the tetragonal β-phase formed as an intermediate phase when the high temperature δ-phase transformed into the stable room temperature monoclinic phase. Previous studies have also monitored the change in δ-phase purity of variously substituted bismuthates over extended periods of time at elevated temperatures, corresponding to typical operating conditions of a SOFC [4–7]. It has been demonstrated that the δ-phase transforms into a variety of phases under these conditions which are correlated to the dopant composition.

Erbium-stabilized bismuthates (12.5–15 mol% Er_2O_3) have shown δ-phase aging into a mixture of the monoclinic, tetragonal and rhombohedral Bi_2O_3 polymorphs [1–3] when annealed at 625 °C for 250 h [8]. Similar phase mixtures were found for a dysprosium-stabilized bismuthate (32.5 mol% Dy_2O_3) when annealed at 815–819 °C for 300–422 h [9]. Terbium-stabilized bismuthates (25 mol% Tb_4O_7) showed the conversion of the δ-phase into the rhombohedral phase [10,11] when annealed at 500 °C for 120 h [5]. The δ-phase yttrium-stabilized bismuthates are significantly less stable when annealed at lower temperatures. Studies by Takahashi et al. [12] showed that annealing an yttrium-stabilized bismuthate (20 mol% Y_2O_3) at 500 °C for 24 h produced significant phase transformations. Yttrium-stabilized bismuthates (25 mol% Y_2O_3) also exhibited a cubic-rhombohedral phase transformation which was observed after annealing at 600 °C for 100–150 h [13,14]. Interestingly, when the yttrium-stabilized bismuthate system (25 mol% Y_2O_3) was co-doped with 2 mol% ZrO_2, phase aging could be inhibited for up to ~1000 h at 600 °C [5,14–17]. Similar inhibition was achieved for ~400 h at 600 °C for the erbium-stabilized bismuthate system (20 mol% Er_2O_3) with the addition of 5 mol% ZrO_2 [18].

Watanabe [19] and Watanabe and Kikuchi [20] postulated that yttrium-'stabilized' δ-phases were not thermodynamically stable but

* Corresponding author. 1 Jan Smuts Avenue, Johannesburg, South Africa.
E-mail address: caren.billing@wits.ac.za (C. Billing).

https://doi.org/10.1016/j.ceramint.2024.07.393
Received 5 March 2024; Received in revised form 18 July 2024; Accepted 27 July 2024
Available online 28 July 2024
0272-8842/© 2024 The Authors. Published by Elsevier Ltd. This is an open access article under the CC BY-NC-ND license (http://creativecommons.org/licenses/by-nc-nd/4.0/).

were rather quenched high temperature stable phases that are only metastable at room temperature. δ-phase solid solutions containing 21.5–23.5 mol% Y_2O_3 were synthesized by solid-state reaction at 850 °C for 20 h [19]. These δ-phased materials were then annealed at 650 °C for >100 h [19] and a rhombohedral phase was formed. 'Stabilized' δ-phases within the same compositional range were synthesized by solid-state reaction at 850 °C for 20 h [20]. These δ-phased materials were then annealed at 650 °C for >160 h and found to completely transform into the rhombohedral phase. Hence the room temperature metastability of the δ-phase Y^{3+}-substituted bismuthate system was proposed. Annealing the δ-phase at 650 °C is, however, likely to promote the cubic-to-rhombohedral phase transformation.

These studies do not, however, provide sufficient detail on the ambient stability of the δ-phase which is essential to evaluate the suitability of these materials as SOFC electrolytes. The phase stability under ambient conditions plays a role when a device is idle or in storage. Thus, while being essential to the successful functioning of a material in a device, ambient metastability is often overlooked. This is done for the first time in this work where changes in the phase purity of 'stabilized' δ-phase materials were monitored upon storing under ambient conditions for extended periods of time. Moreover, the metastable behaviour of several bismuthate materials comprising δ+β-phase mixtures at different stages in the synthesis are also compared when kept under these conditions. Two strategies to enhance the ambient, long-term stability of the δ-phase are also investigated.

2. Materials and methods

2.1. Synthesis and sample preparation

2.1.1. Synthesis of $(Bi_{1-x}Y_x)_2O_3$

All samples of the $(Bi_{1-x}Y_x)_2O_3$ (yttrium substituted Bi_2O_3 – YSB) system were prepared by means of a citrate sol-gel process [21]. Stoichiometric amounts of $Bi(NO_3)_3{\cdot}5H_2O$ (99.99 % pure, Sigma-Aldrich) and $Y(NO_3)_3{\cdot}6H_2O$ (99.8 % pure, Sigma-Aldrich) were dissolved in acetic acid (98 % pure, MK Chemical, 99 %) under moderate heating and stirring. Aqueous solutions were avoided to prevent the hydrolysis of Bi^{3+} [21]. Excess citric acid (ACS reagent, Sigma-Aldrich) was added, and the resulting mixture evaporated under constant stirring to form a metal complex precursor gel. The dried gel was calcined at 450 °C for 18 h. The material was slow-cooled in the furnace (~ 1 °C min^{-1}) to room temperature and then ground into a fine powder. A portion of the calcined sample was kept aside (named YSB$^{\#}$), while the rest was further annealed at 750 °C for 8 h. Both the calcined and further annealed samples were investigated in this case. Additionally, two unique batches of annealed samples of identical composition were prepared and are labelled as batch **A** and batch **B**.

2.1.2. Preparation of YSB pellets

Pellets of the annealed YSB materials were prepared by mixing the powders with a minimal amount of 2 % polyvinyl alcohol aqueous solution (as a binder) and thereafter dried at 120 °C for 20 min. The resulting powder was uniaxially pressed at 100 kPa into pellets using a 5 mm diameter die to produce pellets of ~0.85 mm thickness. The pellets were heated at 250 °C for 4 h to remove the binder and then sintered at 750 °C for 4 h.

2.2. Powder X-ray diffraction

Powder diffractograms of the calcined YSB$^{\#}$ and annealed YSB materials were collected at the Pair-Distribution Function (PDF) beamline 28-ID-1 (λ = 0.1671 Å) at the National Synchrotron Light Source II (NSLS-II). Each 2D diffractogram was collected for 30 s and then reduced into 1D diffraction data using Fit2D [22]. Powder X-ray diffractograms of pelletized samples were collected on a Bruker D2 Phaser using Fe filtered CoK_α radiation (λ = 1.7887 Å) and that for samples annealed under varying atmospheres were collected on a Bruker D8 advance using Ni filtered CuK_α radiation (λ = 1.5404 Å). Identical 27.5YSB samples were heated to ~700 °C at ~1 °C/min under air or N_2 atmospheres and diffractograms were collected before and after heating under each atmosphere. The final diffractogram collected for each aged sample was collected at the PDF beamline described above. To allow for easy comparison of diffractograms measured using different wavelength X-rays, the intensities were plotted against the momentum transfer (Q) rather than 2θ, where $Q = \{4\pi \sin(2\theta/2)\}/\lambda$. All diffractograms were collected at room temperature. Phase identification of diffractograms was done using Bruker AXS DIFFRAC.EVA V4.2 linked to the crystallography open database (COD) [23]. Rietveld refinement of the diffractograms was done using Bruker AXS TOPAS-Academic Version 6 [24]. For the refinements of all the diffractograms collected, the instrument resolution function (IRF) [25] was determined using NIST 660a (LaB_6). For the calibration of all instruments, the IRF was described using the Thompson Cox Hastings (TCHZ) Pseudo-Voigt function [26] with the divergence-related asymmetry effects described in an empirical way using the simple axial model [25]. In each refinement, the parameters refined were the scale factors, selected corrections, and lattice parameters. Atomic positional parameters were fixed to those published for the respective crystal structures and atomic thermal parameters were fixed to reasonable values.

3. Results and discussion

3.1. Investigating the ambient phase stability of the 450 °C calcined YSB$^{\#}$ materials

The calcination step involves the volatilisation of organic components (introduced in the sol-gel synthetic procedure) resulting largely in the formation of metal oxide phases. This is an intermediate step in the synthesis (hence the samples are labelled YSB$^{\#}$). Analysis of the calcined (at 450 °C for 18 h) precursor gels with 10–27.5 % Y^{3+} content (i.e., 10-27.5YSB$^{\#}$) indicated phase mixtures of β-tetragonal ($P4_2$/nmc, SG #137), δ-cubic ($Fm\bar{3}m$, SG #225) and rhombohedral ($R\bar{3}m$, SG #166) substituted bismuth oxide, as well as an orthorhombic bismuth subcarbonate phase ($Imm2$, SG #44). The latter two phases were minor phases and have previously been detected in as-synthesized YSB samples [27]. The crystal structure of bismuth subcarbonate ($Bi_2O_2CO_3$), more commonly known as the mineral bismutite, was first reported by Grice in 2002 [28]. This structure comprises alternating layers of $(Bi_2O_2)^{2+}$ and isolated $(CO_3)^{2-}$ planar groups (Fig. 1) [29]. In general, for the as synthesized materials, the cubic phase content increased as the Y^{3+} concentration increased (from 38 % for 10YSB$^{\#}$ to 92 % for 27.5YSB$^{\#}$) and the tetragonal phase content decreased (from 60 % for 10YSB$^{\#}$ to 8 % for 27.5YSB$^{\#}$) as shown in Table 1. Small amounts of the rhombohedral and bismuth subcarbonate phases were present, except in 27.5YSB$^{\#}$, the material with the highest dopant concentration.

When these calcined materials were stored in powder form under ambient conditions for extended periods of time, spontaneous phase transformations readily occurred (Fig. 2) and were quantified using Rietveld refinement analysis of the diffraction data (Table 1). As an example, the Rietveld analysis of the calcined 10YSB$^{\#}$ material aged for 35 months is shown in Fig. 3. For the samples with relatively low Y^{3+} concentrations (10, 12.5 and 15YSB$^{\#}$), similar phase transformations were evident over the 35-month period, even though the tetragonal phase was initially more dominant for 10YSB$^{\#}$ and the cubic phase was initially more dominant for 12.5 and 15YSB$^{\#}$. A decrease in cubic and tetragonal phase content (less so for the tetragonal phase) was directly correlated to a significant increase in the orthorhombic subcarbonate phase content, while the minor rhombohedral phase content remained largely unchanged. It should be noted that the accuracy of the quantitative analysis of these minor phases is limited. The initial source of carbon which leads to the carbonate content is unknown, but three

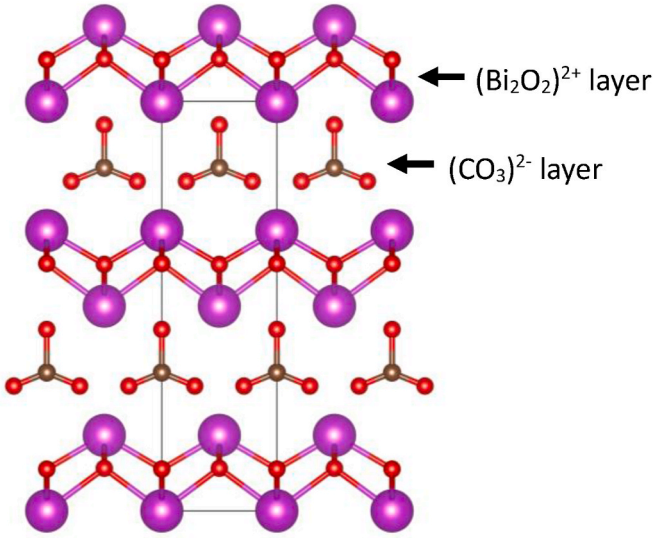

Fig. 1. Crystal structure of bismuth subcarbonate ($Bi_2O_2CO_3$). Purple, bronze and red spheres represent bismuth, carbon and oxygen ions, respectively [28]. (For interpretation of the references to colour in this figure legend, the reader is referred to the Web version of this article.)

Table 1
Variation of the phase composition for the series of YSB# materials calcined at 450 °C when stored under ambient conditions.

Sample Months aged	Phase composition (weight %)			
	Cubic ($Fm\bar{3}m$)	Tetragonal ($P4_2$/nmc)	Rhombohedral ($R\bar{3}m$)	Orthorhombic subcarbonate ($Imm2$)
10YSB#				
0	38.0	60.3	0.9	0.8
11	32.8	59.4	2.0	5.8
24	27.1	46.2	1.6	25.2
35	19.7	51.2	2.0	27.1
12.5YSB#				
0	64.4	32.6	1.2	1.8
11	64.3	30.8	1.4	3.6
24	26.6	22.8	2.3	48.4
35	20.1	13.3	2.2	61.4
15YSB#				
0	60.5	34.1	3.4	2.0
11	48.2	26.0	1.9	23.9
24	37.9	25.7	2.3	34.1
35	22.9	14.2	2.4	60.4
25YSB#				
0	76.1	16.3	2.2	5.5
11	72.8	19.7	1.8	5.7
24	63.2	1.2	25.3	10.4
35	63.4	3.0	23.4	10.2
27.5YSB#				
0	92.4	7.6	0	0
11	85.3	2.3	1.9	10.5
24	18.6	5.5	5.5	70.4
35	15.7	4.8	5.6	73.9

* 0 months aged is equivalent to as synthesized.

possibilities are suggested. Firstly, capture of CO_2 from the atmosphere into the structure could occur. However, flowing CO_2 over a 10YSB# calcined sample for a month did not increase the orthorhombic subcarbonate phase content at all, even when done at a slightly elevated temperature of 80 °C. Secondly, there could be residual carbonaceous combustion products left due to incomplete calcination which would not be detected by XRD. It should be noted that there was no visual evidence of carbon itself which, given the high concentrations of subcarbonate phase in the aged samples, would be observed if present. The slow reaction of these products with the metal oxide could result in the bismuth subcarbonate phase. Thirdly, an amorphous subcarbonate phase could form during the calcination step which becomes more crystalline upon standing due to crystallite nucleation and hence is detected by XRD. This was initially thought unlikely since bismuth subcarbonate has been shown to decompose between 300 and 500 °C, but Sheng et al. [30] showed that doping with Ca^{2+} increased the decomposition temperature and reduced the crystallinity. Similar effects could also have occurred with Y^{3+} as the dopant. However, significant amorphous phase content (as seen in these calcined samples) is expected to produce a broad peak in the low Q range of the XRD data [31], but this was not observed for any of the samples investigated.

Different phase transformation behaviour was evident between the samples with higher Y^{3+} concentrations (25YSB# and 27.5YSB#). For 25YSB#, the cubic phase was significantly more stable than the tetragonal phase over 35 months. A substantial increase in the rhombohedral phase content was seen (from 2 % to 23 %), with the orthorhombic subcarbonate phase content almost doubling (from 6 % to 10 %). This tendency towards rhombohedral phase formation for 25YSB# aligns with the findings of Watanabe [19] and Watanabe and Kikuchi [20], who reported the rhombohedral phase to be stable at room temperature for bismuthates containing 21.5–23.5 mol% Y^{3+}. For 27.5YSB#, there was a substantial increase in orthorhombic subcarbonate phase content (from 0 to 74 %), and a dramatic decrease in the cubic phase (from 92 % to 16 %), with more minor changes occurring for the remaining phases. Interestingly, there was a slight increase in tetragonal phase content for 25YSB# between the period of 24 and 35 months and similarly for 27.5YSB# between 11 and 24 months, revealing a dynamic equilibrium across phases.

Collectively, the phase transformations observed indicate that both the cubic and tetragonal phases are metastable at room temperature for these calcined materials and the orthorhombic subcarbonate phase readily formed when stored at room temperature. For 25YSB#, it appeared that the rhombohedral phase is likely to be the room temperature stable phase. There was no trend in the extent of subcarbonate phase formation with respect to the Y^{3+} substitution in the samples. It should be noted that during the synthesis, the most difficult step to control reproducibly is the gel formation step (the step before calcination) which may influence the phase composition and aging of these materials.

3.2. *Investigating the ambient phase stability of the 750 °C annealed YSB materials*

The annealing step reduces defects and enables crystallite growth, thereby moving towards an equilibrium state. The cubic phase bismuthates are commonly synthesized at temperatures of ~700–800 °C [6, 32–35]. The thermal prehistory (i.e., thermal treatments applied during synthesis or preparation) of substituted bismuthates has been shown to affect both the optical [36] and magnetic [37] properties of these materials. In this work, the long-term ambient phase stability of the annealed materials is investigated and compared to that of the calcined materials.

Portions of the calcined samples (investigated in Section 3.1) were immediately ground and further annealed at 750 °C for 8 h (batch **A**). A second set of samples (batch **B**) was prepared for comparison to probe the possibility of incidental trace or amorphous impurity phase/s persisting after being annealed and to gauge the reproducibility of the aging process. The phase composition of the annealed materials, as quantified by Rietveld refinement (Table 2), confirmed that annealing promotes cubic phase formation, and that mainly cubic-to-tetragonal phase conversion occurs. Phase pure cubic samples formed when the Y^{3+} concentration was 25–27.5 mol%.

After storing the annealed powder materials under ambient conditions, they were analysed (after 8 and 20 months for batch **A** and after 14 and 25 months for batch **B**). Spontaneous phase changes were still

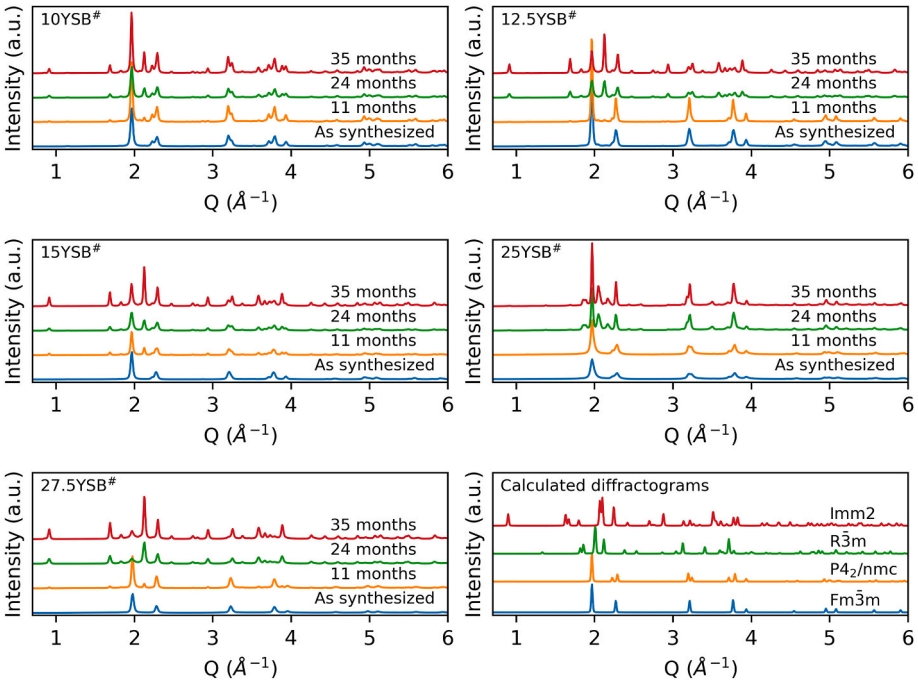

Fig. 2. Diffractograms of the series of YSB# samples calcined at 450 °C collected following their synthesis and after storing the materials in powdered form under ambient conditions for 11, 24 and 35 months are shown. Calculated diffractograms of the respective phases are also given.

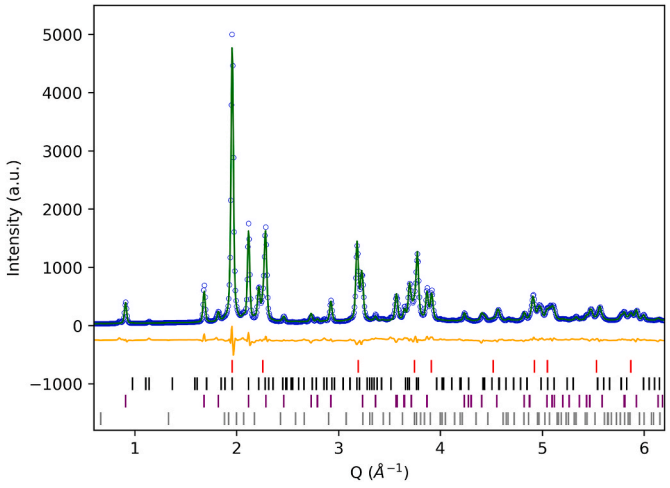

Fig. 3. Diffractogram showing Rietveld refinement analysis for the 10YSB# material calcined at 450 °C after aging under ambient conditions for 35 months (R_{wp} = 7.7, R_{ex} = 7.8, GoF = 1.0). The observed (blue), calculated (green) and the difference (orange) patterns are shown. Miller indices corresponding to the cubic (red), tetragonal (black), orthorhombic (purple) and rhombohedral (grey) phases are shown with tick marks. (For interpretation of the references to colour in this figure legend, the reader is referred to the Web version of this article.)

evident but occurred to a smaller extent as compared to the calcined samples (Table 2). As an example, Rietveld analysis results are presented in Fig. 4 for the 20-month aged 10YSB-**A** material (i.e. from batch **A**).

For the 10YSB samples the initial phase compositions were similar for the two batches and showed a mixture of cubic and tetragonal phases, with more of the latter phase being present (on average 48 % cubic and 52 % tetragonal). Upon aging, cubic-to-tetragonal phase transformation was observed at an average rate of 0.8 % per month over the period studied (Table 2, Fig. 5). This indicates the metastability of the cubic phase for low Y^{3+} content materials. 10YSB-**B** additionally

Table 2
Variation in the phase composition of the YSB series of samples for batches **A** and **B** (calcined at 450 °C and then annealed at 750 °C) when stored under ambient conditions.

Sample Months aged	Phase composition (weight %)							
	Cubic ($Fm\bar{3}m$)		Tetragonal ($P4_2/nmc$)		Rhombohedral ($R\bar{3}m$)		Orthorhombic subcarbonate ($Imm2$)	
	A	B	A	B	A	B	A	B
10YSB								
0	46.6	48.9	53.4	51.1	0	0	0	0
8	37.5	–	62.5	–	0	–	0	–
14	–	37.8	–	61.0	–	1.3	–	0
20	30.0	–	70	–	0	–	0	
25	–	29.2	–	68.1	–	2.7	–	0
12.5YSB								
0	68.7	37.2	31.3	60.7	0	2	0	0
8	56.9	–	43.1	–	0	–	0	–
14	–	24.0	–	69.7	–	4.8	–	1.5
20	51.1	–	48.9	–	0	–	0	–
25	–	22.0	–	72.9	–	2.8	–	2.3
15YSB								
0	86.0	86.1	14.0	13.9	0	0	0	0
8	73.3	–	21.6	–	4.4	–	0.8	–
14	–	60.5	–	10.4	–	0.6	–	28.5
20	66.0	–	27.8	–	5.1	–	1.1	–
25	–	53.8	–	16.4	–	0.6	–	29.2
25YSB								
0	100	100	0	0	0	0	0	0
8	98.4	–	0	–	0.3	–	1.3	–
14	–	96.8	–	0	–	1	–	2.2
20	96.4	–	0	–	0.6	–	3	–
25	–	96.8	–	0	–	0.3	–	2.9
27.5YSB								
0	100	100	0	0	0	0	0	0
8	96.2	–	0	–	1.3	–	2.6	–
14	–	94.7	–	0	–	1.1	–	4.2
20	94.8	–	0	–	0.9	–	4.3	–
25	–	90.6	–	0	–	4.8	–	4.7

* 0 months aged is equivalent to as synthesized.

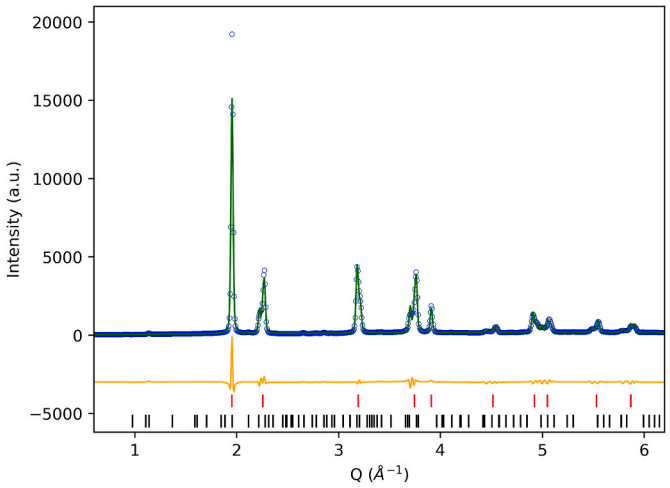

Fig. 4. Diffractogram showing Rietveld refinement analysis for the 10YSB-**A** material annealed at 750 °C after aging under ambient conditions for 20 months (R_{wp} = 13.9, R_{ex} = 5.1, GoF = 2.7). The observed (blue), calculated (green) and difference (orange) patterns are shown. Miller indices corresponding to the cubic (red) and tetragonal (black) phases are shown with tick marks. (For interpretation of the references to colour in this figure legend, the reader is referred to the Web version of this article.)

showed minor rhombohedral phase formation upon aging which was not anticipated for samples with low Y^{3+} concentrations.

The initial phase compositions for the two batches of 12.5YSB were inexplicably very different (cubic content of 69 % for **A** and 38 % for **B**), with 12.5YSB-**B** giving the expected results based on the trend of increasing cubic phase content with increasing Y^{3+} content. The reason for this discrepancy in unknown. Nonetheless, the aging of both samples were studied out of interest. Both batches also showed cubic-to-tetragonal phase transformation upon aging, with 12.5YSB-**B** also showing minor rhombohedral and orthorhombic subcarbonate phase formation. The decrease in rhombohedral phase content between 14 and 25 months indicates that the rhombohedral phase is also metastable under ambient conditions for this composition. This variation in phase aging behaviour is clearly related to the distinct initial phase composition in this case.

For the 15YSB samples the initial phase compositions for the two batches were identical and consisted of a mixture of cubic (86 %) and tetragonal (14 %) phases. However, the aging behaviour for these two samples was remarkably different. As before, mainly the cubic-to-tetragonal phase transition occurred for 15YSB-**A**, with minor rhombohedral and orthorhombic subcarbonate phases also forming. For 15YSB-**B** the cubic-to-tetragonal transition still occurred, but a significant quantity of the orthorhombic subcarbonate phase appeared (29 % after 14 months). In contrast, only 1 % of the subcarbonate phase was present after 20 months for 15YSB-**A**. In this case the variation in phase aging behaviour is not directly linked to the initial crystallite phase composition. It is suspected that more remnant phases were present in this sample, be it as residual carbonaceous material (carbon specifically was not observed microscopically) or amorphous subcarbonates. Since all samples in batch **B** were synthesized at the same time, and calcined and annealed in the same furnace (which had been calibrated), it can only be speculated that there is a cooler spot in the furnace where this sample was placed, or that the gelation step was not sufficiently driven to completion for this sample. This study looked solely at the crystalline content of the samples, but clearly a more in-depth investigation is required based on the presented results.

For 25YSB and 27.5YSB, all samples initially showed a pure cubic phase and no tetragonal phase formation occurred upon aging. However, minor transitions to the rhombohedral phase did occur, which was more pronounced for the higher substituted 27.5YSB samples (Table 2, Fig. 6). Additionally, 3–5% of the orthorhombic subcarbonate phase was present after 25 months. On average the rate of decrease in the cubic phase content was 0.16 % and 0.32 % per month for 25YSB and 27.5% YSB, respectively. These more highly substituted samples are more stable under ambient conditions and, based on this limited study, it appears that substitution with 25 % Y^{3+} optimises cubic phase stability.

Overall, the metastability of δ-phase bismuthates is evident in the annealed YSB and especially in the calcined YSB$^{\#}$ samples reported in this work. Partial transformation to the rhombohedral phase was

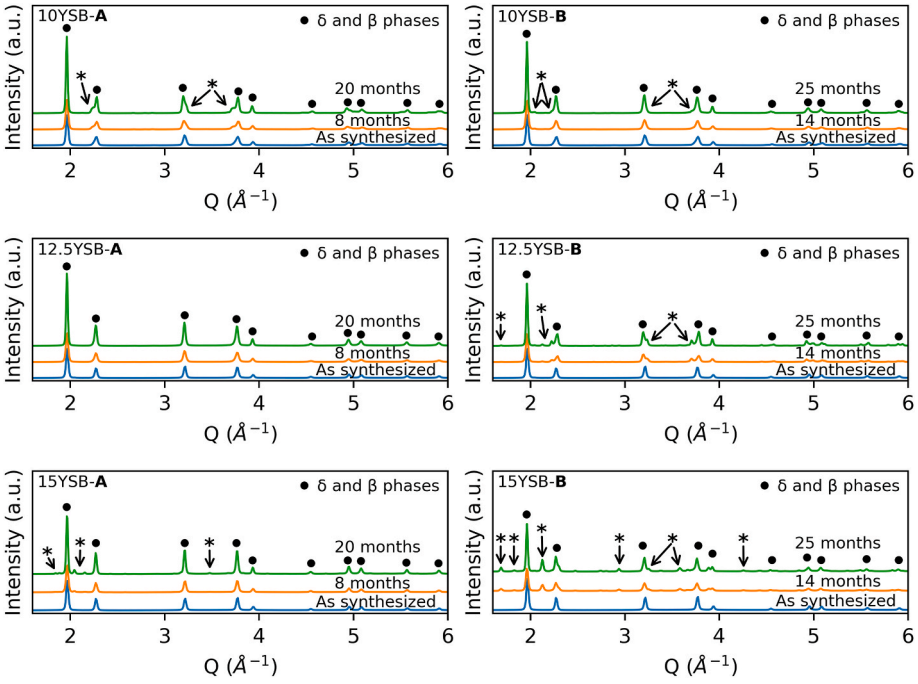

Fig. 5. Diffractograms of the 10-15YSB samples annealed at 750 °C for batches **A** and **B** are compared. The diffractograms were collected after synthesis and then after storing in powdered form under ambient conditions. Prominent changes are indicated by * symbols.

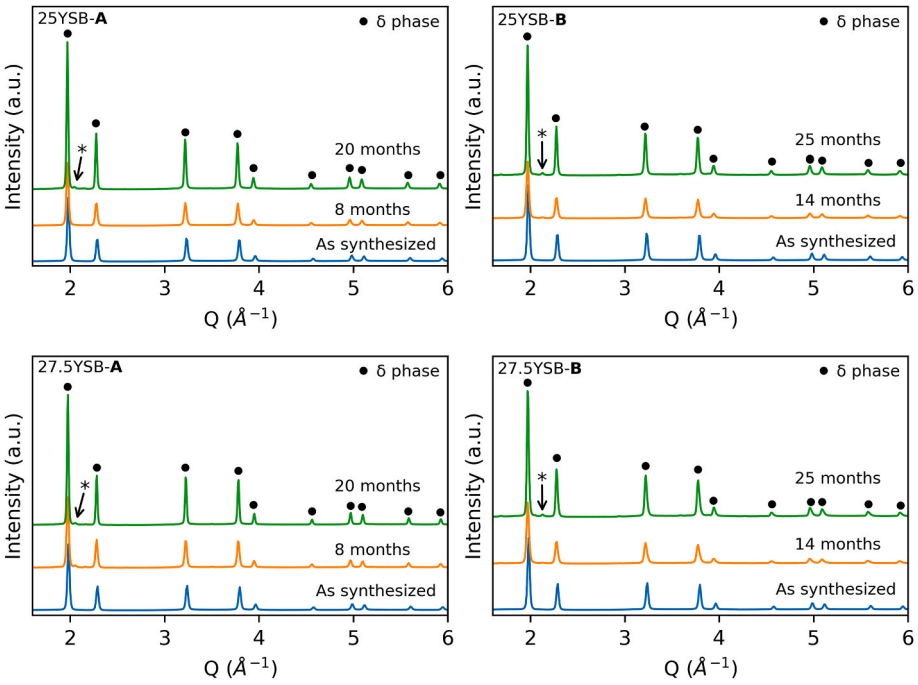

Fig. 6. Diffractograms of the 25 and 27.5YSB samples annealed at 750 °C for batches **A** and **B** are compared. The diffractograms were collected after synthesis and then after storing in powdered form under ambient conditions. Prominent changes are indicated by * symbols.

observed to varying extents. This phase is proposed by Watanabe [19] to be the true stable room temperature phase for Bi_2O_3 solid solutions containing 21.5–23.5 mol% Y_2O_3, but was not exclusively found in samples close to that concentration range in this work. Watanabe [38] also reported that the rhombohedral phase of several substituted bismuth oxides containing Ca^{2+}, Sr^{2+} or Ba^{2+}, synthesized using the conventional solid-state route, had limited stability when exposed to a humid atmosphere at room temperature. Under these conditions, the rhombohedral phase decomposed into monoclinic α-Bi_2O_3 together with an 'unknown' phase. Based on their presented data, it cannot be confirmed that this unknown phase is bismuth subcarbonate. In this work, the orthorhombic bismuth subcarbonate phase readily formed under ambient conditions for the calcined and several annealed samples with varying Y^{3+} concentrations. This was significantly more prevalent in the calcined materials, supporting the hypothesis that occurrence of this phase is due to trace residual carbonaceous or amorphous material.

The ambient metastability is not limited to the Y_2O_3-substituted bismuth oxide system or to materials synthesized via the citrate sol-gel method. $(Bi_{1-x-y}Dy_xEr_y)_2O_3$ (DESB) and $(Bi_{1-x-y-z}Dy_xEr_yW_z)_2O_3$ (DEWSB) systems, synthesized using both the sol-gel and solid-state methods, also exhibited bismuth subcarbonate formation (see Section S2 in the Supporting Information). In the solid-state synthesis, acetone was introduced when grinding hence a carbon source is present in this process too. The formation of the subcarbonate phase was found to be reversible with the phase disappearing on reheating.

3.3. Investigating the effect of pelletisation on the ambient phase stability of YSB materials

In SOFC devices, the electrolyte used is in the form of a densified, sintered layer [39]. Valuable insights can thus be gained from investigating the ambient phase stability of densified materials, approximated as thin sintered pellets in this work. Both 10YSB and 27.5YSB were looked at due to the large dopant concentration difference resulting in distinct phase compositions for these materials. For this, annealed materials were again synthesized (i.e., batch **C**) and a portion of the powder samples was used to make the sintered pellets. The powder and pellet samples were stored under identical ambient conditions and then analysed via laboratory based PXRD after 14 and 20 months, respectively. From the diffractograms (Fig. 7) it is noted that the cubic phase content of 10YSB-**C** stored as a powder, significantly decreased over 14 months, with an average rate of cubic-to-tetragonal phase conversion of 1.8 % per month (Table 3). When pelletized, the cubic phase purity significantly increased, and the average rate of cubic-to-tetragonal phase conversion was about 0.04 % per month over the 20-month period. For the 27.5YSB-**C** material, no phase transformations were evident in either powder or pellet form over the same timeframes. No rhombohedral or orthorhombic phase content was detected in any of these samples, most likely due to the limited resolution of the laboratory instrument.

The results for the 10YSB-**C** sample indicate that the pellet preparative methodology, which includes application of high-pressure followed by sintering thereby causing densification and average grain size growth, promotes the formation of the cubic phase and enhances its ambient long-term stability. It is noteworthy that the X-rays have only superficial penetration of the pellet, thus the diffractograms do not necessarily represent the bulk material, but rather a surface layer (~10–20 μm [40]). If the phase transformations are induced by the atmospheric conditions, it is expected that the surface would be most affected.

3.4. Investigating the effect of the annealing atmosphere on the ambient phase stability of δ-phase YSB materials

The effect of the annealing atmosphere on the long-term ambient phase stability of phase pure cubic 27.5YSB material was also investigated. A 27.5YSB material was again synthesized and annealed at 750 °C as before (i.e., batch **D**). Two separate portions of this material were reheated to ~700 °C at ~1 °C/min, one in air and the other in a nitrogen atmosphere, then slow cooled to room temperature in the respective atmospheres at ~1 °C/min, and finally stored under ambient conditions for 11 months. The sample heated in air showed significant formation of the rhombohedral phase after 11 months (~6.2 %), whereas the sample that was heated under a nitrogen atmosphere showed only trace rhombohedral phase formation (Fig. 8). The apparent lower phase

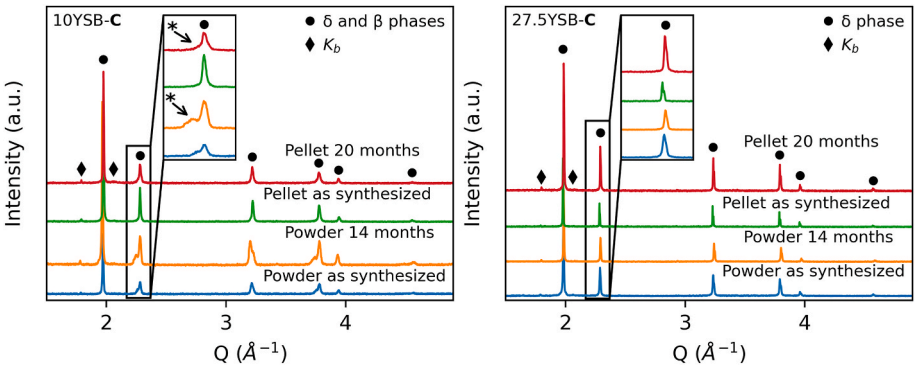

Fig. 7. Laboratory-based diffractograms of 10YSB-**C** and 27.5YSB-**C** annealed at 750 °C showing the varying effects on phase stability under ambient conditions when materials are stored in powder and pelletized forms. The diffractograms collected after materials were synthesized and then stored in powdered or pelletized form under ambient conditions are indicated. Prominent changes observed for the 10YSB powder and pellet are indicated by * symbols in the inset.

Table 3
Variation in phase composition of the 10YSB-**C** sample stored as an annealed powder and a sintered pellet.

10YSB-C	Cubic ($Fm\ \bar{3}\ m$) phase %	Tetragonal ($P4_2$/nmc) phase %	% change/ month
Powder as synthesized	49.1	50.9	1.8
Powder after 14 months	23.3	76.7	
Pellet as synthesized	98.3	1.7	0.04
Pellet after 20 months	97.6	2.4	

stability of the material heated in air could be attributed to formation of trace amorphous rhombohedral phase content during the thermal cycle, which then slowly crystallizes under ambient conditions. Additionally, loss of oxygen from the structure could occur when the material is heated under the nitrogen atmosphere. This decrease in oxygen content could enhance the stability of the δ-phase under ambient conditions, resulting in the reduced rate of rhombohedral phase formation. This suggests that additional heating under an inert atmosphere could be beneficial to the long-term phase stability of cubic YSB materials.

4. Conclusion

Longer-term stability studies have revealed that substituted Bi_2O_3 ceramics undergo spontaneous phase transformations even under ambient conditions. For materials annealed at 750 °C, those doped with 10–15 % Y^{3+} mainly underwent cubic-to-tetragonal phase transformations. Formation of the rhombohedral phase occurred to a small extent in most materials with 10–27.5 % Y^{3+} content, with the 25 % doped sample displaying the highest cubic phase stability. These transformations were seen to a much larger extent in all samples that had only been calcined at 450 °C, showing the importance of the annealing step. The formation of an orthorhombic bismuth subcarbonate phase upon aging under ambient conditions was also far more pronounced in the calcined materials than the annealed materials. Although the source of this phase is not fully understood, it is speculated that it is due to either incomplete combustion of organic components leading to further reaction, or trace subcarbonate phase being present initially as an amorphous phase which crystallises with time resulting in its detection by XRD. The organic components are added as complexing agents in the sol-gel synthesis or as wetting agents in the case of the solid-state synthetic procedures. This ties in with the subcarbonate phase being more prevalent in materials that were only calcined. Further investigation into the bismuth subcarbonate phase formation mechanism using techniques such as SEM-EDS and Raman spectroscopy. Additionally, quantifying the amorphous phase content of these materials by more advanced approaches, such as adding a crystalline internal standard to samples when doing XRD measurements [31], is also required.

In general, the aging behaviour is not fully reproducible as variations were observed between batches of what initially appeared to be identical samples. This points to possible subtle differences in the thermal prehistory playing a role. Furthermore, it was shown that pelletisation of 10YSB appreciably enhanced the cubic phase purity and reduced aging when compared to the powdered sample. Annealing of 27.5YSB in a nitrogen atmosphere revealed increased ambient phase stability of the cubic phase over extended periods of time.

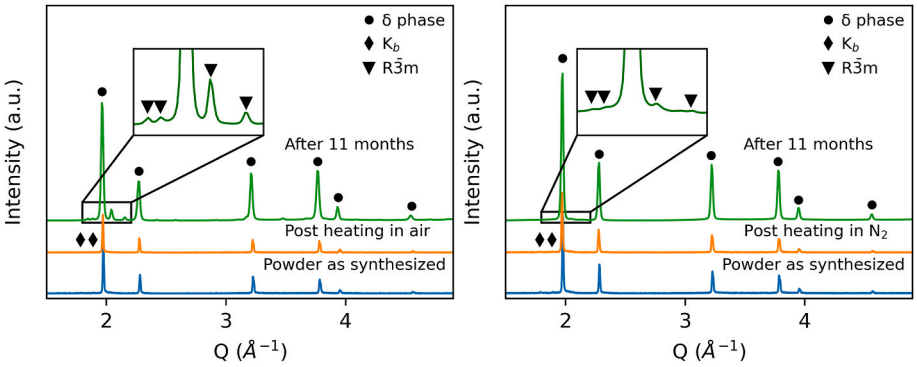

Fig. 8. Diffractograms of 27.5YSB annealed at 750 °C showing the effect of the heating atmosphere on the ambient phase stability of the δ-phase. The diffractograms collected after the material was synthesized, heated under air and N_2 atmospheres and then stored under ambient conditions are indicated. Prominent rhombohedral phase peaks are indicated in the inset.

CRediT authorship contribution statement

Mathias A. Kiefer: Writing – review & editing, Writing – original draft, Methodology, Investigation, Formal analysis, Data curation, Conceptualization. **Sikhumbuzo M. Masina:** Methodology, Investigation, Formal analysis, Data curation, Conceptualization. **Caren Billing:** Writing – review & editing, Writing – original draft, Supervision, Resources, Project administration, Investigation, Conceptualization. **Daniel Olds:** Validation, Data curation. **David G. Billing:** Validation, Supervision, Resources, Project administration, Funding acquisition, Formal analysis, Conceptualization.

Declaration of competing interest

The authors declare that they have no known competing financial interests or personal relationships that could have appeared to influence the work reported in this paper.

Acknowledgements

The authors acknowledge financial support for their research from the National Research Foundation (NRF, South Africa, Grant No: 141966) and Department of Science and Innovation (DSI, South Africa, Grant UID: 41292), as well as the University of the Witwatersrand. This research used beamline 28-ID-1 of the National Synchrotron Light Source II, a U.S. Department of Energy (DOE) Office of Science User Facility operated for the DOE Office of Science by Brookhaven National Laboratory under Contract No. DE-SC0012704.

Appendix A. Supplementary data

Supplementary data to this article can be found online at https://doi.org/10.1016/j.ceramint.2024.07.393.

References

[1] H.A. Harwig, On the structure of bismuthsesquioxide: the α, β, γ and δ-phase, Z. Anorg. Allg. Chem. 444 (1978) 151–166, https://doi.org/10.1002/zaac.19784440118.
[2] H.A. Harwig, A.G. Gerards, The polymorphism of bismuth sesquioxide, Thermochim. Acta 28 (1979) 121–131, https://doi.org/10.1016/0040-6031(79)87011-2.
[3] C.N.R. Rao, G.V.S. Rao, S. Ramdas, Phase transformations and electrical properties of bismuth sesquioxide, J Phys Chem 73 (1968) 672–675. http://pubs.acs.org/doi/abs/10.1021/j100723a031.
[4] A.M. Azad, S. Larose, S.A. Akbar, Bismuth oxide-based solid electrolytes for fuel cells, J. Mater. Sci. 29 (1994) 4135–4151, https://doi.org/10.1007/BF00414192.
[5] D.W. Jung, K.T. Lee, E.D. Wachsman, Terbium and tungsten co-doped bismuth oxide electrolytes for low temperature solid oxide fuel cells, J. Korean Ceram. Soc. 51 (2014) 261–264, https://doi.org/10.4191/kcers.2014.51.4.260.
[6] A.B. Stambouli, E. Traversa, Solid oxide fuel cells (SOFCs): a review of an environmentally clean and efficient source of energy, Renew. Sustain. Energy Rev. 6 (2002) 433–455, https://doi.org/10.1016/S1364-0321(02)00014-X.
[7] J.W. Fergus, Electrolytes for solid oxide fuel cells, J. Power Sources 162 (2006) 30–40, https://doi.org/10.1016/j.jpowsour.2006.06.062.
[8] M.J. Verkerk, K. Keizer, A.J. Burggraaf, High oxygen ion conduction in sintered oxides of the Bi_2O_3-Er_2O_3 system, J. Appl. Electrochem. 10 (1980) 81–90, https://doi.org/10.1007/BF00937342.
[9] A. Watanabe, Polymorphic transformation of δ-Bi_2O_3 stabilized with Ln_2O_3 (Ln=Sm, Eu, Gd, Tb, and Dy) into a new phase with a C-type rare-earth oxide-related structure, Solid State Ionics 79 (1995) 84–88, https://doi.org/10.1016/0167-2738(95)00035-5.
[10] A.G. Jolley, R. Jayathilake, E.D. Wachsman, Optimizing rhombohedral Bi_2O_3 conductivity for low temperature SOFC electrolytes, Ionics 25 (2019) 3531–3536, https://doi.org/10.1007/s11581-019-02920-x.
[11] T. Takahashi, H. Iwahara, Y. Nagai, High oxide ion conduction in sintered Bi_2O_3 containing SrO, CaO or La_2O_3, J. Appl. Electrochem. 2 (1972) 97–104, https://doi.org/10.1007/BF00609125.
[12] T. Takahashi, H. Iwahara, T. Arao, High oxide ion conduction in sintered oxides of the system Bi_2O_3-Y_2O_3, J. Appl. Electrochem. 5 (1975) 187–195, https://doi.org/10.1007/BF01637268.
[13] K.Z. Fung, A.V. Virkar, D.L. Drobeck, Massive transformation in the Y_2O_3-Bi_2O_3 system, J. Am. Ceram. Soc. 77 (1994) 1638–1648, https://doi.org/10.1111/j.1151-2916.1994.tb09768.x.
[14] K.Z. Fung, A.V. Virkar, Phase stability, phase transformation kinetics, and conductivity of Y_2O_3-Bi_2O_3 solid electrolytes containing aliovalent dopants, J. Am. Ceram. Soc. 74 (1991) 1970–1980, https://doi.org/10.1111/j.1151-2916.1991.tb07817.x.
[15] S. Arasteh, A. Maghsoudipour, M. Alizadeh, A. Nemati, Effect of Y_2O_3 and Er_2O_3 co-dopants on phase stabilization of bismuth oxide, Ceram. Int. 37 (2011) 3451–3455, https://doi.org/10.1016/j.ceramint.2011.04.136.
[16] T. Chou, L.D. Liu, W.C.J. Wei, Phase stability and electric conductivity of Er_2O_3-Nb_2O_5 co-doped Bi_2O_3 electrolyte, J. Eur. Ceram. Soc. 31 (2011) 3087–3094, https://doi.org/10.1016/j.jeurceramsoc.2011.04.016.
[17] K. Huang, M. Feng, J.B. Goodenough, Bi_2O_3-Y_2O_3-CeO_2 solid solution oxide-ion electrolyte, Solid State Ionics 89 (1996) 17–24, https://doi.org/10.1016/0167-2738(96)00260-3.
[18] K.Z. Fung, H.D. Baek, A.V. Virkar, Thermodynamic and kinetic considerations for Bi_2O_3-based electrolytes, Solid State Ionics 52 (1992) 199–211, https://doi.org/10.1016/0167-2738(92)90106-Y.
[19] A. Watanabe, Is it possible to stabilize δ-Bi_2O_3 by an oxide additive? Solid State Ionics 41 (1990) 889–892, https://doi.org/10.1016/0167-2738(90)90145-H.
[20] A. Watanabe, T. Kikuchi, Cubic-hexagonal transformation of yttria-stabilized δ-bismuth sesquioxide, $Bi_{2-2x}Y_{2x}O_3$ (x=0.215-0.235), Solid State Ionics 21 (1986) 287–291, https://doi.org/10.1016/0167-2738%2886%2990191-8.
[21] A.E. Danks, S.R. Hall, Z. Schnepp, The evolution of 'sol-gel' chemistry as a technique for materials synthesis, Mater. Horiz. 3 (2016) 91–112, https://doi.org/10.1039/C5MH00260E.
[22] A.P. Hammersley, FIT2D: a multi-purpose data reduction, analysis and visualization program, J. Appl. Crystallogr. 49 (2016) 646–652, https://doi.org/10.1107/S1600576716000455.
[23] S. Gražulis, D. Chateigner, R.T. Downs, A.F. Yokochi, M. Quirós, L. Lutterotti, E. Manakova, J. Butkus, P. Moeck, A. Le Bail, Crystallography Open Database - an open-access collection of crystal structures, J. Appl. Crystallogr. 42 (2009) 726–729, https://doi.org/10.1107/S0021889809016690.
[24] A.A. Coelho, TOPAS and TOPAS-Academic: an optimization program integrating computer algebra and crystallographic objects written in C++: an, J. Appl. Crystallogr. 51 (2018) 210–218, https://doi.org/10.1107/S1600576718000183.
[25] R.E. Dinnebier, A. Leineweber, J.S.O. Evans, Rietveld Refinement Practical Powder Diffraction Pattern Analysis Using Topas, first ed., Walter de Gruyter GmbH, Berlin/Boston, 2019.
[26] P. Thompson, D.E. Cox, J.B. Hastings, Rietveld refinement of debye-scherrer Synchrotron X-ray data from Al_2O_3, J. Appl. Crystallogr. 20 (1987) 79–83, https://doi.org/10.1107/S0021889887087090.
[27] M.A. Kiefer, C. Billing, R.M. Erasmus, W.M. Mogodi, D.G. Billing, A detailed investigation of the structural stability, ionic conductivity and in situ δ-phase formation of $Y_xBi_{2-x}O_\delta$, S. Afr. J. Chem. 76 (2022) 111–119, https://doi.org/10.17159/0379-4350/2022/v76a16.
[28] J.D. Grice, A solution to the crystal structures of bismutite and beyerite, Can. Mineral. 40 (2002) 693–698, https://doi.org/10.2113/gscanmin.40.2.693.
[29] H. Huang, N. Tian, S. Jin, Y. Zhang, S. Wang, Syntheses, characterization and nonlinear optical properties of a bismuth subcarbonate $Bi_2O_2CO_3$, Solid State Sci. 30 (2014) 1–5, https://doi.org/10.1016/j.solidstatesciences.2014.01.010.
[30] S. Sheng, S. Jin, K. Cui, Thermal decomposition of nanostructured bismuth subcarbonate, Materials 13 (2020) 1–10, https://doi.org/10.3390/ma13194287.
[31] I.C. Madsen, N.V.Y. Scarlett, A. Kern, Description and survey of methodologies for the determination of amorphous content via X-ray powder diffraction, Z. Kristallogr. 226 (2011) 944–955, https://doi.org/10.1524/zkri.2011.1437.
[32] N.M. Sammes, G.A. Tompsett, H. Näfe, F. Aldinger, Bismuth based oxide electrolytes— structure and ionic conductivity, J. Eur. Ceram. Soc. 19 (1999) 1801–1826, https://doi.org/10.1016/S0955-2219(99)00009-6.
[33] T. Takahashi, H. Iwahara, Oxide ion conductors based on bismuthsesquioxide, Mater. Res. Bull. 13 (1978) 1447–1453, https://doi.org/10.1016/0025-5408(78)90138-1.
[34] E.D. Wachsman, Development of a lower temperature SOFC, ECS Trans. 25 (2009) 783–788, https://doi.org/10.1149/1.3205595.
[35] P. Shuk, H.D. Wiemhöfer, U. Guth, W. Göpel, M. Greenblatt, Oxide ion conducting solid electrolytes based on Bi_2O_3, Solid State Ionics 89 (1996) 179–196, https://doi.org/10.1016/0167-2738(96)00348-7.
[36] M.A. Girsova, S.V. Firstov, T.V. Antropova, Structural and optical properties of the bismuth-containing quartz-like glasses, J Phys Conf Ser 541 (2014), https://doi.org/10.1088/1742-6596/541/1/012022.
[37] E.A. Kravchenko, Magnetism of bismuth (III) oxide-based compounds, Solid State Phenom. 233–234 (2015) 113–116. https://doi.org/10.4028/www.scientific.net/SSP.233-234.113.
[38] A. Watanabe, Phase stability of $Bi_{0.765}Sr_{0.235}O_{1.383}$-type bismuth mixed oxides with hexagonal symmetry, Solid State Ionics 35 (1989) 281–283, https://doi.org/10.1016/0167-2738%2889%2990309-3.
[39] H. Kawamoto, Research and development trends in solid oxide fuel cell materials, Science & Technology Trends (2008) 52–70. https://core.ac.uk/download/pdf/236667437.pdf.
[40] A.T. Fry, Residual Stress Measurement: XRD Depth Profiling Using Successive Material Removal, National Physical Laboratory Report No: MATC(MN)034, UK, 2002. http://eprintspublications.npl.co.uk/id/eprint/2494.